1999

Resistivity, thermopower and the correlation to infrared active vibrations of Mn1.56Co0.96Ni0.48O4 spinel films sputtered in an oxygen partial pressure series

Rand Dannenberg
S. Baliga
R. J. Gambino, *State University of New York at Stony Brook*
Alexander H. King, *State University of New York at Stony Brook*
A. P. Doctor

Resistivity, thermopower and the correlation to infrared active vibrations of $Mn_{1.56}Co_{0.96}Ni_{0.48}O_4$ spinel films sputtered in an oxygen partial pressure series

Rand Dannenberg, S. Baliga, R. J. Gambino, A. H. King, and A. P. Doctor

Citation: J. Appl. Phys. **86**, 514 (1999); doi: 10.1063/1.370760
View online: http://dx.doi.org/10.1063/1.370760
View Table of Contents: http://jap.aip.org/resource/1/JAPIAU/v86/i1
Published by the American Institute of Physics.

Resistivity, thermopower and the correlation to infrared active vibrations of $Mn_{1.56}Co_{0.96}Ni_{0.48}O_4$ spinel films sputtered in an oxygen partial pressure series

Rand Dannenberg[a)]
Presently at BOC Coating Technology, 2700 Maxwell Way, Fairfield, California 94533

S. Baliga
General Monitors, Lake Forest, California

R. J. Gambino and A. H. King
Materials Science Department, State University of New York, Stony Brook, New York

A. P. Doctor
Servo Corporation of America, Westbury, New York

(Received 8 December 1998; accepted for publication 25 March 1999)

$Mn_{1.56}Co_{0.96}Ni_{0.48}O_4$ spinel was sputter deposited using a series of oxygen partial pressures. Electrical resistivity versus temperature and thermopower versus temperature measurements at each oxygen partial pressure were made. The variations of the thermopower and resistivity with oxygen partial pressure are consistent with a change in the ratio of $Mn^{3+}$to Mn^{4+} cations, which occurs due to changes of oxygen content of the material. The weak temperature dependence of the thermopower indicates small polaron hopping is the charge transport mechanism. Combining the models of Mott and Schnakenberg to analyze the transport data, we find that the Debye temperature (or frequency) is an increasing function of the oxygen partial pressure used during sputtering. The calculated shift in the Debye frequency from the resistivity is consistent with the observed shift in the fundamental infrared active lattice vibrations from Fourier transform infrared spectroscopy and Raman spectroscopy. © *1999 American Institute of Physics.* [S0021-8979(99)04913-0]

I. INTRODUCTION: THERMOPOWER AND POLARON CONDUCTIVITY

Mn-Co-Ni-O spinel, owing to its large temperature dependent resistivity, is an attractive ternary system for thermistor applications, and for infrared detecting bolometers. The materials resistivity can be changed by altering the relative contents of the metallic species, producing a range of spinel structured solid solutions. $Mn_{1.56}Co_{0.96}Ni_{0.48}O_4$ is a composition of some specific importance because it is very near the resistivity minimum for the ternary oxide.[1]

The objectives of this study are as follows: (1) Characterize the transport properties, specifically, thermopower and resistivity versus temperature, when the oxygen content of this material is varied. The oxygen content is varied by sputter depositing the material in a series of oxygen partial pressures. (2) Identify the transport mechanism of the sputtered films of varying stoichiometry. (3) Rationalize our method of analysis and interpretation by observing the shift of infrared restrahlen bands and Raman active lattice vibrations with the oxygen partial pressure during the deposition process. The theory connecting thermopower, resistivity and the Debye temperature is introduced below. We relate the theory to our oxide in this section, as well.

The thermopower of a semiconductor is given by the general expression[2–5]

$$Q=(k/e)(\ln(N/n)+S), \tag{1}$$

where n is the carrier concentration which may be temperature dependent, N is the limiting value of that concentration, and S is an entropy term which is usually very small and is neglected.[5] If that concentration is thermally activated and $n=N\exp(-E_S/kT)$ then

$$Q=(k/e)(E_S/kT+A), \tag{2}$$

where E_S is the thermopower activation energy and A is a constant which depends on the scattering mechanism, and is usually between 1 and 4.[3] In a band gap semiconductor, $E_S=E_C-E_F$ if the material is n type where e is negative, and if p type $E_S=E_F-E_V$ where e is positive. E_C, E_V, and E_F are the energies of the conduction band, valence band, and Fermi level.

Small polaron carriers have a temperature dependent concentration which goes as[6]

$$N_P\sim(\cosh(E_S/2kT))^{-2}. \tag{3}$$

Equation (3) predicts that the polaron concentration should become temperature independent at high temperature.

Many oxides display thermally activated conduction with activation energies much smaller than their band gaps. These oxides have temperature dependent resistivities often due to the thermally activated hopping of small polarons between states that are localized about cation sites of mixed valance. Systems where the ratio of Mn^{3+} and Mn^{4+} are varied with a second dopant have been studied, and when

a)Author to whom correspondence should be addressed; Electronic mail: rdannen314@aol.com

conduction occurs by hopping of small polarons between Mn^{3+} and Mn^{4+} sites, the relation between the concentrations $[Mn^{4+}]$, $[Mn^{3+}]$ and thermopower is

$$Q=(k/e)\ln\left(\frac{1}{\beta}\frac{[Mn^{3+}]}{[Mn^{4+}]}\right). \tag{4}$$

In Eq. (4), $\beta=5/4$, and is a spin degeneracy factor.[7] Note that this is not dependent on temperature, since at sufficiently high temperature, the number of carriers is fixed by the chemistry.

The transport in Mn-Co-Ni-O spinel is believed to affected most by the ratio of the Mn^{3+} and Mn^{4+}. A cation distribution proposed by Yokoyama for stoichiometric Mn-Co-Ni-O spinel is shown in Eqs. (5)[8]

$$[{Co^{2+}}_{1.16X}{Mn^{2+}}_{1-1.16X}]$$
$$\times[{Ni^{2+}}_{1-X}{Co^{3+}}_{0.84X}{Mn^{4+}}_{1-X}{Mn^{3+}}_{1.16X}]{O^{2-}}_4. \tag{5}$$

The composition of the specific oxide under study is very close to Eq. (5) when $X=0.48$. That is, the sum of the subscripts of the Co is 0.96 in our oxide, and is also in Eq. (5) when $X=0.48$. Also, the subscript sums of the Mn and Ni in our oxide vary only slightly from Eq. (5) when $X=0.48$.

Let us adjust Yokoyama's distribution to fit more closely to our own by slightly adjusting the Ni^{2+}concentration and the Mn^{3+} and Mn^{4+}concentration, but, leaving the total Co concentration unaltered (since Co in both is 0.96), while preserving charge balance and site balance. The result is

$$[{Co^{2+}}_{0.557}{Mn^{2+}}_{0.443}]$$
$$\times[{Ni^{2+}}_{0.48}{Co^{3+}}_{0.403}{Mn^{4+}}_{0.48}{Mn^{3+}}_{0.637}]{O^{2-}}_4 \tag{6}$$

and so the composition under study would have slightly more Mn^{3+} than Mn^{4+}, placing it in the *p* regime. To wit, $[Mn^{3+}]/[Mn^{4+}]=0.637/0.480=1.32$, and by Eq. (4), should give a thermopower of $+24\mu$V/K. The measured thermopower for the target bulk ceramic is, in fact, about 30 μV/K. Thus, the stoichiometric material is right at the edge of the *p* to *n* transition, since the argument of the natural log in Eq. (4) is equal to 1.06. Slightly more Mn^{4+} and the argument of Eq. (4) will be less than one, resulting in a negative thermopower, or, *n*-type behavior. If the material becomes sufficiently super stoichiometric in oxygen, the Mn^{4+} concentration should rise and the material should show a transition from *p*-type ($Q>0$) to *n*-type ($Q<0$) behavior. Therefore, this specific composition is useful for probing the effects of processing on the chemistry of reactively sputtered material, and as a further test of Yokoyama's conclusions.[8]

For small polarons, it is the *mobility* that is thermally activated at high temperatures, not the density of polarons, which is fixed by the chemistry. The resistivity of small polarons has different limiting functional forms, dependent on the temperature. For the small polaron resistivity ρ, in a plot of $\ln(\rho/T)$ vs $1/T$ for $T\gg\theta_D$ (where θ_D is the Debye temperature) the resistivity activation energy (or slope) is $E_\sigma=W_H+(1/2)W_D+E_S$. $W_H=(1/2)W_P\cdot W_P$. W_P is the potential well depth in which the polaron is self-trapped due to its distortion of the lattice. W_D is the spacing between localized energy levels in its defect ''band'' as derived by Mott.[4] At high temperatures, $W_H\gg W_D$. For $T\ll\theta_D$, there is a drop in the activation energy to the smaller value, W_D. The polaron then behaves as a nearly free carrier with a large effective mass, essentially because at low temperatures it is no longer hopping, but is tunneling between hopping sites (equivalently, tunneling from one localized state into another). For $T\sim\theta_D$, there is a transition in the value of W_H which follows a relationship due to Schnakenberg,[4,9]

$$W_H\rightarrow\frac{W_H\tanh(\theta_D/4T)}{\theta_D/4T} \tag{7}$$

which is approximately

$$W_H\rightarrow W_H(1-\tfrac{1}{3}(\theta_D/4T)^2). \tag{8}$$

Plots of $\ln(\rho/T)$ vs $1/T$ are expected to be linear at high temperature with slope W_H; at intermediate temperatures these plots should have a slight negative second derivative, and at temperatures $T\ll\theta_D$ should essentially have zero slope. Equations (8) and (9) are most meaningful at the onset of the transition at intermediate temperatures, where the deviation from $1/T$ linearity is just beginning. In this study, the data of highest precision is in this region, and it is this region of temperatures which can be used diagnostically to determine the Debye temperature from the resistivity versus temperature dependence.

These ideas are contained in the expression

$$\ln(\rho/T)=\ln(\rho_0/T)+\frac{W_H(T)}{kT}+\frac{W_D}{2kT}+\frac{E_S}{kT}. \tag{9}$$

This is like the often used empirical fit for thermistors $\ln\rho=A_0+A_1/T+A_3T^3$ if the right hand side of Eq. (8) is substituted for $W_H(T)$, except each term now has physical meaning.[10] The author is unaware at this time of any previous discussions on the physical significance of this fit. There have been many fits developed for putting smooth lines through thermistor resistivity versus temperature data with no physical basis.[10–12]

The important diagnostic relation from Eq. (9) is that $W_H+(1/2)W_D=E_\sigma-E_S$ where $E_\sigma$is the slope of the $\ln(\rho/T)$ vs $1/T$ plot. Comparing Eqs. (2) and (9), if $E_\sigma>E_S$ it may be concluded that transport is by small polaron hopping.

The conductivity pre-exponential is given by a diffusional expression (Nernst–Einstein) and is

$$\frac{1}{\rho_0}=\sigma_0=\frac{Ne^2d^2c(1-c)\nu_D}{kT}, \tag{10}$$

where Nc is the concentration of carriers, $N(1-c)$ is the concentration of vacant sites onto which the carriers may hop, N is the total concentration of sites participating in the hopping, e is the electronic charge, d is the jump distance, ν_D is the jump attempt frequency and is usually associated with the Debye frequency.[8] For this system, $Nc=[Mn^{3+}]$ and $N(1-c)=[Mn^{4+}]$.

To summarize, if $E_\sigma>E_S$, this indicates a small polaron hopping mechanism. If E_S appears to go to zero at high temperatures in a plot of the thermopower versus temperature, this means that the small polaron concentration has saturated. At low temperatures, the slope of the resistivity gives W_D+E_S, and if this is zero, then W_D is zero at all temperatures. If the zero slope is not observed at low tem-

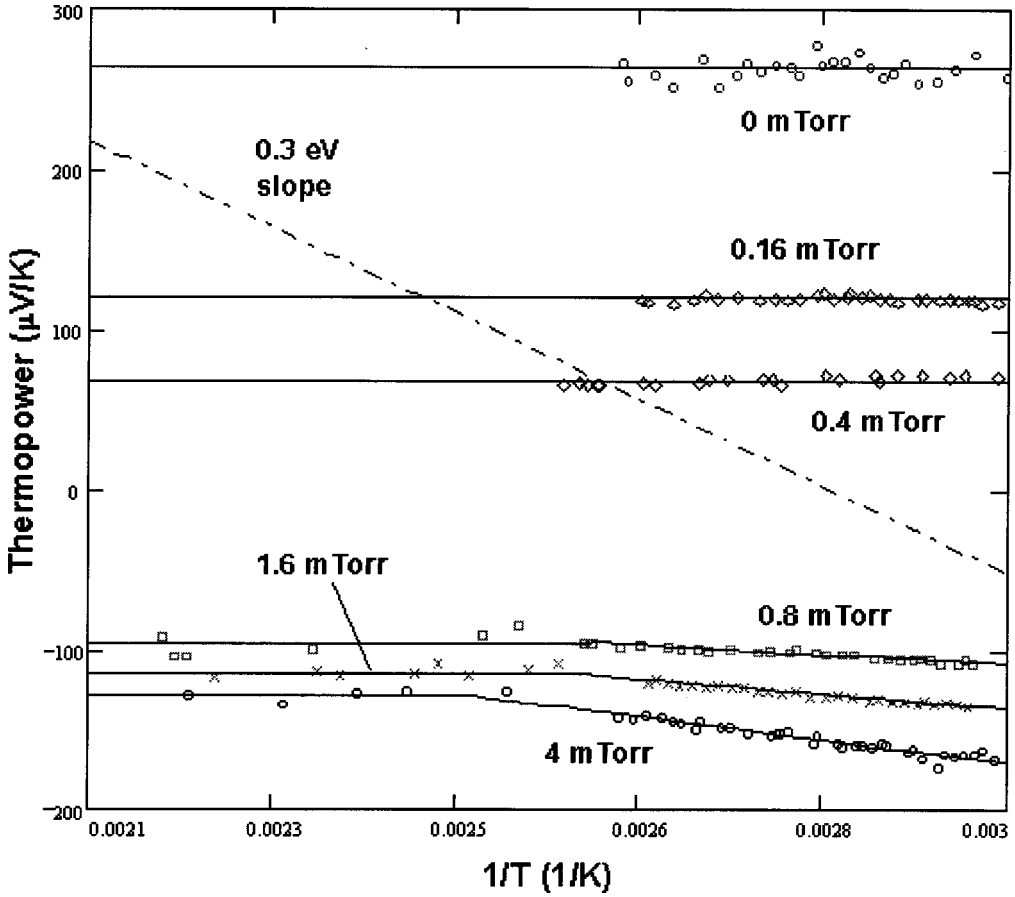

FIG. 1. Thermopower as a function of temperature ($1/T_{\mathrm{mod}}$) for samples sputtered in six different oxygen partial pressures. The dotted line is how Q should vary if $E_\sigma = E_S$ indicating that $E_\sigma > E_S$ and the carriers are small polarons. Oxygen partial pressures of 0, 0.16, 0.4, 0.8, 1.6, and 4 mTorr are shown in descending order.

perature, then $E_\sigma(\text{low } T) - E_S(\text{low } T) = W_D$. If the thermopower cannot be measured at sufficiently low temperature, then W_D cannot separate. Typically $W_D \ll W_H$ in the intermediate and high temperature regimes.

II. FILM DEPOSITION, PHASE COMPOSITION, AND METAL CONTENT

Films were sputtered in 0, 0.16, 0.4, 0.8, 1.6, and 4 mTorr oxygen partial pressures onto insulating steatite porcelain substrates, with 4 mTorr corresponding to a partial pressure of 10% of oxygen. The total $Ar+O_2$ pressure was 40 mTorr for all cases. Details of the deposition process have been published earlier by Baliga, Jain, and Zachovsky.[13–15] Films were deposited by rf magnetron sputtering using a sintered ceramic target.

X-ray diffraction (XRD) showed the target material to be single-phase cubic spinel with 56% Mn, 32% Co, and 16% Ni. Films were also observed to be a single-phase spinel. X-ray energy dispersive spectroscopy showed, for all films, that the metallic composition varied by less than 2% from the target for each species. Both the lattice constant (8.35–8.42 Å) and the composition of the metals in the films did not show trends which could be associated with the oxygen partial pressure during deposition, and so could not be used diagnostically to determine the oxygen content in the films. The measured variation of the metal content in the films was too small to account for the large changes in thermopower.

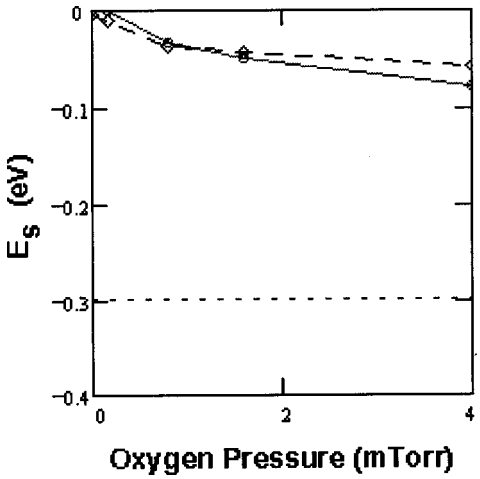

FIG. 2. Thermopower activation energy vs oxygen partial pressure. The values are shown as negative to indicate the slope of the thermopower vs $1/T_{\mathrm{mod}}$. The dotted line at 0.3 eV is the activation energy for conduction. The first two data points are p-type ($Q>0$). The remaining n-type ($Q<0$) samples show an increase in E_S with oxygen partial pressure at lower temperatures. The solid and dotted lines are from two measurements of the same sample, which shows the repeatability of the measurement.

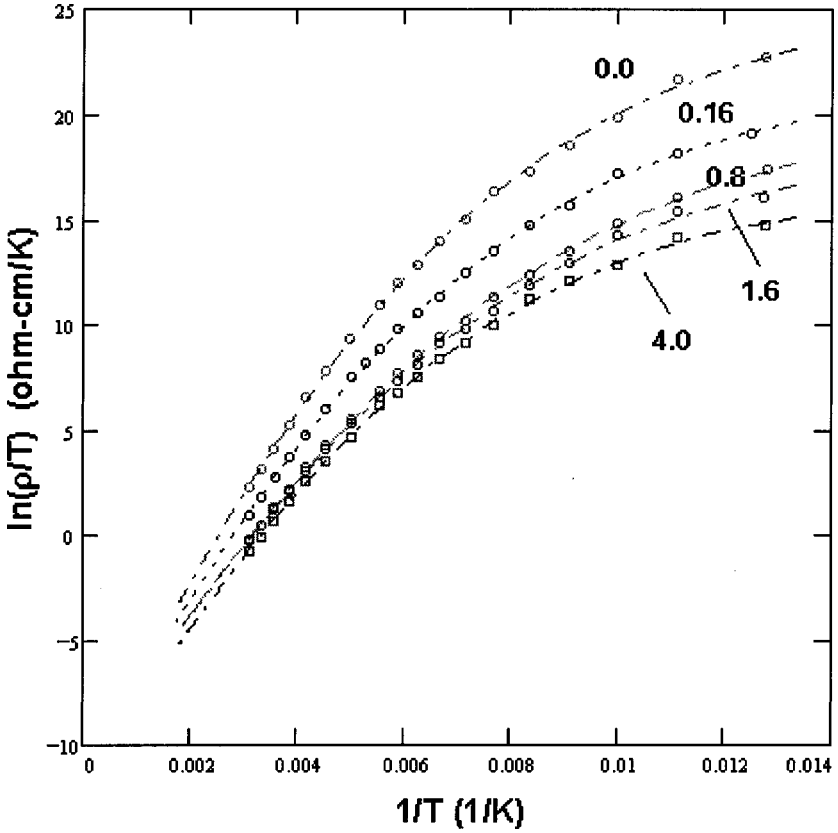

FIG. 3. Fits to the low temperature resistivity data between 77 to 320 K assuming $E_S=0$ in all cases. The curves are for the 0, 0.16, 0.8, 1.6, and 4 mTorr specimens, in descending order. Note flattening at low temperature.

III. TRANSPORT MEASUREMENTS

A. Measurement of thermopower

Gold contacts were evaporated onto the specimens, delineating a 5 mm by 5 mm ''active'' area. One side of the specimen was heated on a hot plate (the hot side or directly heated side), while the other side was in contact with a large metallic heat sink (the cold side or indirectly heated side). Data were collected as both sides cooled, approaching the same temperature. The temperature gradient was measured using two contact thermocouples at the boundaries of the evaporated gold contact electrode and active areas. Point probes at the boundaries were used to measure the voltage. The voltage was amplified by a factor of 100 with a properly calibrated, zeroed, linear amplifier.

The temperature difference across the specimens was as high as 100 °C for the highest temperatures measured, and 20 °C was roughly the lowest. The large gradient was required to generate a measurable thermoelectric voltage, presumably owing to the low mass of the films. Generally, temperature gradients as low as 5 °C produce significant thermoelectric voltages in bulk samples. The effect of a fairly large temperature gradient on the calculated thermopower must be evaluated, as we are trying to find the thermopower as a function of temperature. Consider $S=\Delta V/\Delta T$ being reported at the average temperature, T_{ave}. $S(T_{\text{ave}})$ is an approximation to the true thermopower $Q(T)$. From the definition of the thermopower, we have the thermovoltage for a thermal gradient that is position dependent over a length L

$$\Delta V=\int_0^L Q(T(x))\frac{dT}{dx}dx\approx\Delta T\frac{1}{L}\int_0^L Q(T(x))dx=\Delta T\cdot Q_{\text{ave}}, \tag{11}$$

where the approximation results from assuming that the temperature gradient is linear across the active area with a constant slope $\Delta T/L$ with $\Delta T=T_{\text{cold}}-T_{\text{hot}}$. T_{hot} and T_{cold} are the temperatures of the hot side and cold sides. Equation (2) with the temperatures replaced by the linearly varying form $T(x)=T+(\Delta T/L)x$ gives $Q(T(x))$, and when this is substituted into the integral of Eq. (11) for the Q_{ave}, we find

$$Q_{\text{ave}}=(k/e)\left(\frac{E_S}{k\Delta T}\ln\left(1+\frac{\Delta T}{T_{\text{hot}}}\right)+A\right). \tag{12}$$

If T_{hot} is sufficiently larger than T_{cold} then $Q_{\text{ave}}=S$, and $1/T_{\text{ave}}$ is numerically equal to $\ln(1+\Delta T/T_{\text{hot}})/\Delta T$. We will call this product $1/T_{\text{mod}}$. This treatment shows that the thermopower activation energy can be determined from knowing Q_{ave} and $1/T_{\text{mod}}$ with a fairly large gradient. Knowing E_S, A, and with $1/T_{\text{mod}}$ numerically equal to $1/T_{\text{ave}}$, plots of Q_{ave} vs $1/T_{\text{mod}}$ [Eq. (12)] are numerically identical to plots of Q vs $1/T$ [Eq. (2)]. An additional advantage of a large temperature difference is that the signal is unlikely to be dominated by amplifier dc offset drifts.

There was no measurable thermoelectric voltage using the uncoated steatite substrates with gold contacts, and no change in the film resistivity before and after the ther-

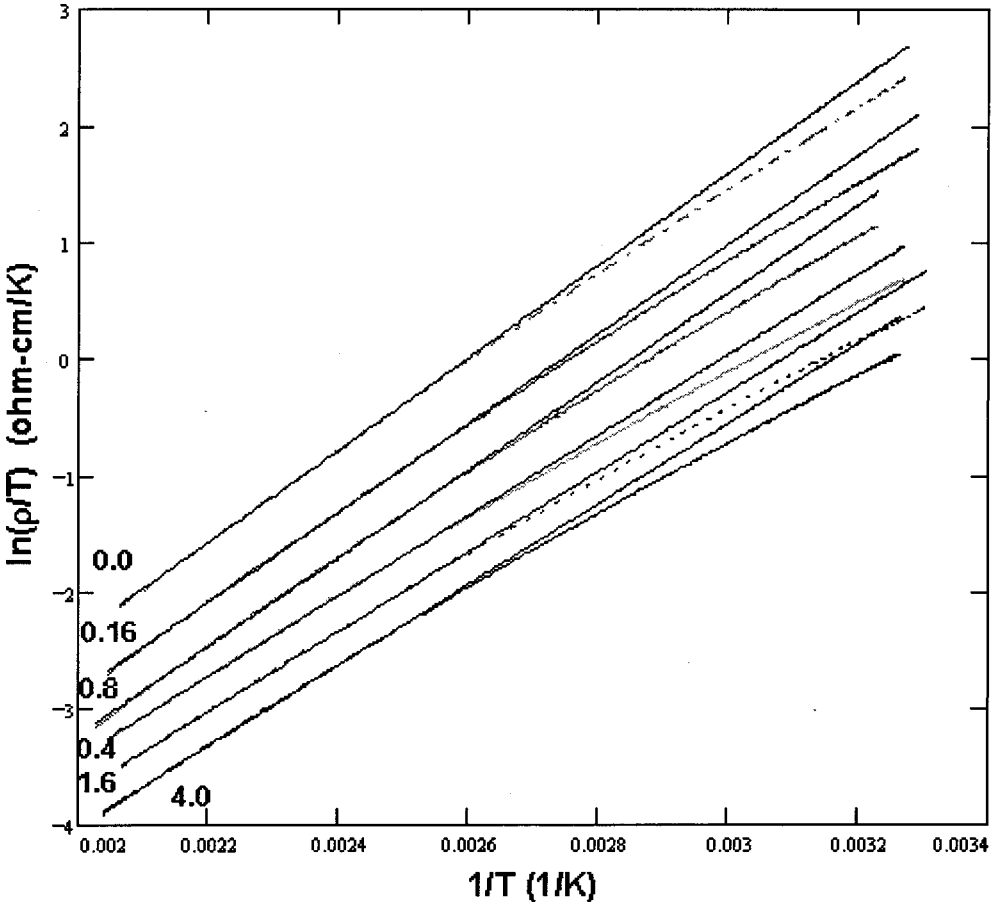

FIG. 4. The $\ln(\rho/T)$ vs $1/T$ plots of high precision resistivity-temperature data between 300 and 525 K, for 0, 0.16, 0.8, 0.8, 1.6, and 4 mTorr oxygen partial pressure, in descending order. The straight lines show the deviation from linearity at lower temperatures, and more linear fit at higher temperatures. The region at $1/T > 0.0026\ \mathrm{K}^{-1}$ was used to calculate Table I.

mopower measurements. Probing the temperature along the length of the specimen showed that the temperature gradient was approximately linear.

B. Measurement of resistivity

The material resistivity varies by six orders of magnitude over the temperature range from 77 to 320 K. To keep the resistance below $10^{14}\ \Omega$, which is the range of the electrometer used for the measurement, the specimens of the thermopower measurement were modified. Instead of a 5 mm by 5 mm active area, a 5 mm by 25 μm area was used. The 25 μm long strip was made by stretching a 25 μm diam bonding wire across the specimen, and using it as a mask for the gold evaporation. This resulted in a precisely defined active area.

Samples were mounted on a cold finger in a vacuum dewar, evacuated to less than 5 μm pressure. A two-point method was used to measure the resistance, and reversing the polarity at the electrometer resulted in no measurable differences, indicating that thermoelectric effects did not contribute. The temperature was measured with a precision calibrated silicon diode sensor. The diode was mounted permanently next to the specimen on the cold finger. After pouring liquid nitrogen into the dewar and reaching 77 K, the sample temperature could be programmed with a digital temperature controller. Equilibrium temperatures could be reached by a combination of controlling the area of thermal contact of the nitrogen to the finger and/or with the controller.

For the resistivity measurement between 300 and 525 K, specimens with active area of 5 mm by 5 mm were suspended in florinert electronic fluid. This was done to prevent oxygen evolution of the sample, to provide a large mass so that the data could be taken under near equilibrium conditions, and to reduce temperature gradients. Resistance versus temperature data was taken on cooling to room temperature from 525 K over a 14 h period by an automated data acquisition system, collecting 500 data points per run. Temperature was measured with a low mass, calibrated thermocouple floating in the fluid about 2 mm from the specimen active area. Again, reversal of the polarity of the ohmmeter resulted in no measurable difference, and there was no difference in the data from run to run on the same specimen.

Resistance measurements were converted to resistivity with knowledge of the active area defined by the masking procedure when the gold was evaporated, and by measurement of the film thickness. A calibrated JEOL T-200 scanning electron microscope was used to measure the film thickness, which ranged from 2 to 8 μm.

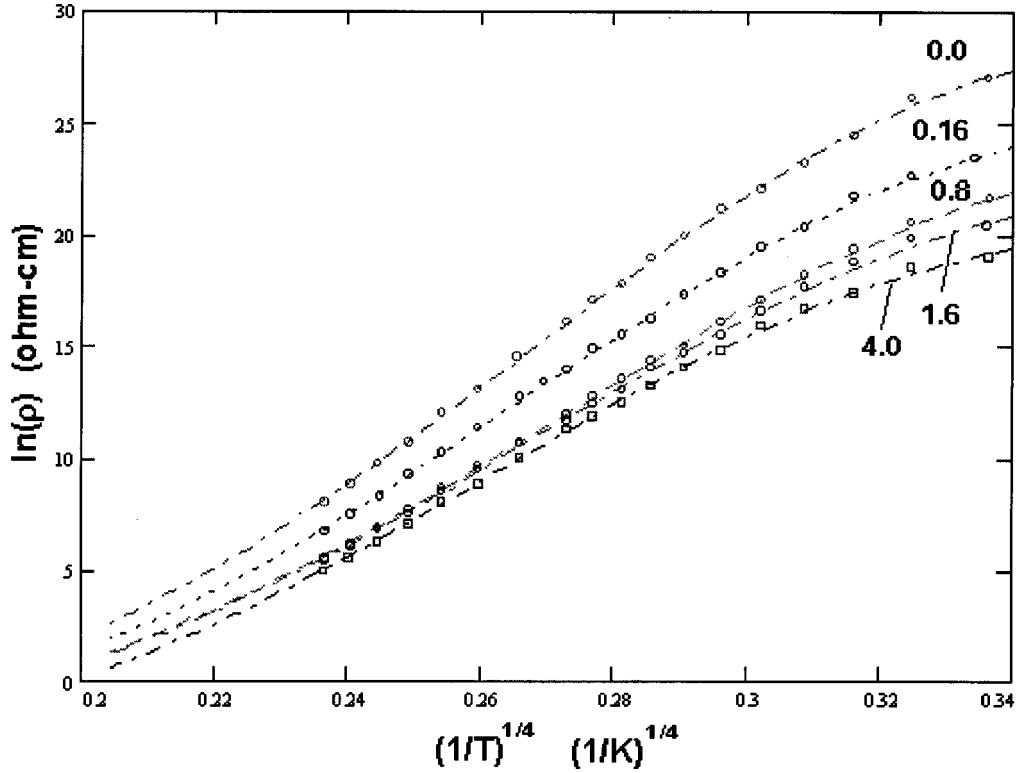

FIG. 5. Fit of low temperature data to the $T^{-1/4}$ VRH law for five oxygen partial pressures. If the law were obeyed the fit would be linear.

IV. THERMOPOWER AND RESISTIVITY RESULTS

A. Thermopower

Since E_S does not contain the polaron term, but E_σ does, then if $E_\sigma > E_S$, conduction is due to polarons, and this has been observed in MnO, CoO, and many substituted manganates, although the results are more controversial for NiO.[2,3]

Evidence of the small polaron carrier in this material is given in Fig. 1. $E_\sigma > E_S$ at all the temperatures measured. In addition, it is seen that the samples sputtered on 0 through 0.4 mTorr oxygen partial pressures are *p* type, and the higher partial pressures are *n* type. The higher density data was taken in a range of average temperature between 30 and 120 °C to prevent oxygen evolution in or out of the sample. The measurement was carried out in air with a T_{hot} temperature under 140 °C for the 0 and 0.16 mTorr specimens since they can change resistivity by a factor of about -20% in air within 1 min at 220 °C. The four higher oxygen partial pressure samples do not evolve as quickly, and so the measurement could be extended to an average temperature of about 200 °C. There was no measurable change in resistivity after the measurement for any of the specimens.

A slight negative slope is seen to develop in the samples sputtered in the higher oxygen partial pressures in these figures, at lower temperatures. If the slope/drop-off were due to an activation term, then positive thermopowers should have positive slope, and negative thermopowers should have negative slope.[2–4] The three *p*-type ($Q>0$) specimens have negligible slope. The three *n* types ($Q<0$) have negative slopes that increase with oxygen partial pressure, but which are less than $0.23E_\sigma$ in all cases (Fig. 2). Also, the temperature dependence appears to go to zero at higher temperatures, which may indicate a saturating polaron density.[6]

B. Resistivity data 77 to 525 K

Figures 3 and 4 show the characteristics of the small polaron carrier: more linear behavior at higher temperatures, followed by a deviation in nonlinearity with a negative second derivative, and the activation energy (slope) approaching a small value at low temperature. Since the slope is nonzero at low temperatures and we do not have the ability to measure the thermopower to low temperatures, W_D cannot be deconvoluted in this study.

As of this writing, the author has been unable to reproduce the $T^{-1/4}$ behavior observed by Baglia *et al.* at low temperature as demonstrated by the fits of Figs. 5 and 6 which are poor for that mechanism, and also the $T^{-1/2}$ mechanism.[1,15] These as-deposited films at high temperatures are not variable range hopping (VRH) as demonstrated by the thermopower temperature dependence, which is very small. $Ni_xFe_{3-x}O_4$ with $x>0.4$ is an example that obeys the $T^{-/14}$ law at low temperature (20–100 K), but has a very temperature dependent thermopower in that same range.[16]

The low temperature mechanism in as-deposited films reported by Baliga and Jain may not have been variable range hopping, but the fit was good enough that it could not be discounted.[15] Further work or reinterpretation is needed to resolve this discrepancy. Low temperature thermopower measurements would shed some light.

Using Eqs. (7) and (9), the thermopower activation energies E_S, the resistivity data of Fig. 4 for $1/T$

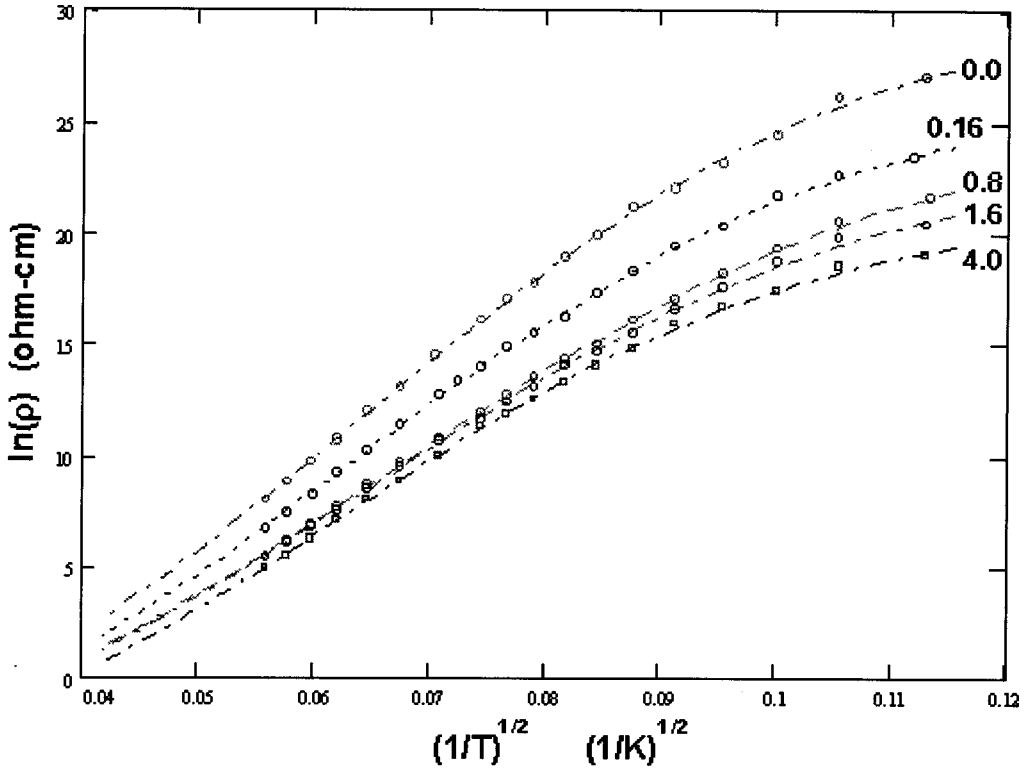

FIG. 6. Fit of the low temperature data to the $T^{-1/2}$ law for five oxygen partial pressures. If the law were obeyed the fit would be linear.

$>0.0026\ \mathrm{K}^{-1}$, and assuming that W_D is small, the Debye temperature and polaron activation energy W_H can be calculated. This region of temperature is used because resistivity and thermopower data exist for all specimens, and, the onset of the resistivity versus $1/T$ curvature begins here. The right hand side of Eq. (7) is substituted for $W_H(T)$ in Eq. (9).

The results are summarized in Table I. The trends in the pre-exponent and activation energy persist whether the thermopower activation energy is included or not, although somewhat more noisily, Table II.

V. RAMAN SPECTRA AND FOURIER TRANSFORM INFRARED (FTIR) SPECTROSCOPY REFLECTANCE MEASUREMENTS

Optical specimens were prepared by sputtering under conditions similar to those already described, onto doubly polished silicon substrates 235 μm thick.

The Raman spectra of Fig. 7 were collected on a Nicolet 960 FT-Raman spectrometer under the following conditions: (1) 4 W laser power at the sample, (2) 512 sample scans, (3) 2 cm^{-1} resolution, and (4) Ge detector. The collection time was 13 min per sample. The Fourier transform infrared (FTIR) reflections of Fig. 8 were performed on a Nicolet 550 FTIR.

Note from Table III that the restrahlen peaks from FTIR reflection, and Raman peaks shift to higher wave number (or frequency) with increasing oxygen partial pressure. Note that the Debye temperature (or frequency) also shifts to higher values with oxygen partial pressure.

VI. DISCUSSION

Carriers are small polarons as evidenced by: (1) weakly temperature dependent thermopower quantified by $E_S \ll E_\sigma$. (2) A resistivity versus temperature relation which shows an approach to temperature independence at low temperature

TABLE I. Results of curve fitting Eqs. (9) and (7) to the data in Fig. 4 in the region where $1/T > 0.0026\ \mathrm{K}^{-1}$ to resolve the θ_D. Thermopower Q is from the temperature independent regions. The right hand side of Eq. (7) is substituted for $W_H(T)$ in Eq. (9).

	E_S(eV)	W_H (eV)	θ_D (K)	$\ln(\rho_0/T)$ (Ω cm/K)	$Q(\mu V/K)$	Carrier type
0 mTorr	0	0.372	552	−10.55	264	P
0.16 mTorr	0	0.372	619	−11.193	120	P
0.4 mTorr	0	0.362	625	−11.384	64	P
0.8 mTorr	0.034	0.292	635	−10.821	−95	N
1.6 mTorr	0.05	0.282	681	−11.145	−115	N
4 mTorr	0.08	0.256	741	−11.313	−128	N

TABLE II. Results of curve fitting Eqs. (7) and (9) to the entire region of data between 300 and 525 K (Fig. 4) assuming $E_S = 0$. Thermopower Q is from the temperature independent regions.

	E_S(eV)	W_H (eV)	θ_D (K)	$\ln(\rho_0/T)$ (Ω cm/K)	$Q(\mu V/K)$	Carrier type
0 mTorr	0	0.389	610	−11.162	264	P
0.16 mTorr	0	0.387	664	−11.556	120	P
0.4 mTorr	0	0.387	689	−11.885	64	P
0.8 mTorr	0	0.347	668	−11.199	−95	N
1.6 mTorr	0	0.345	669	−11.442	−115	N
4 mTorr	0	0.352	695	−11.877	−128	N

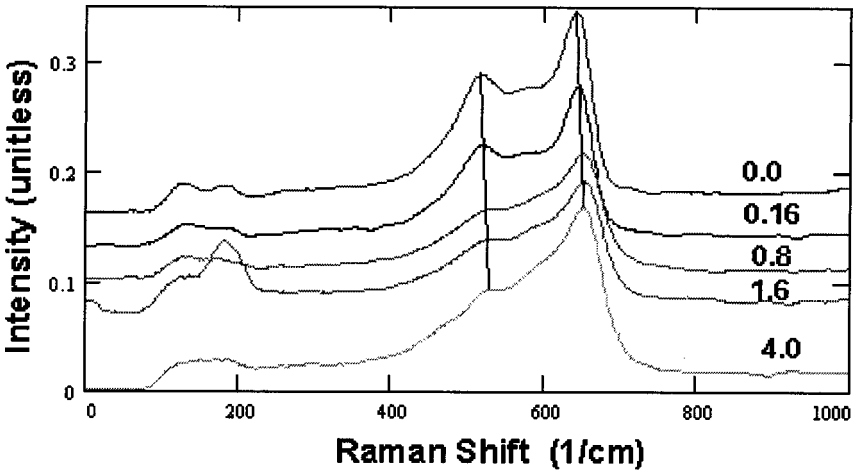

FIG. 7. Raman spectra of the oxygen partial pressure series 0, 0.16, 0.8, 1.6, 4 mTorr shown in descending order. Note shift of peaks to higher wave number from top to bottom with increasing oxygen. Data are spaced for clarity.

and an approach to exponential behavior at high temperature. (3) Poor fits to the $T^{-1/2}$ or $T^{-1/4}$ variable range hopping laws.

It is expected that since the films retain the spinel structure, the ratio of Mn^{3+} to Mn^{4+} will decrease on passing through a range of stoichiometries, from oxygen substoichiometry to superstoichiometry, since a higher average metallic oxidation state will be required for charge balance. This is sufficient to explain the change on the sign of Q with the oxygen partial pressure, Eq. (4).

Note from Table I and Table II that there is a rapid drop in the activation energy at the transition from *p*-type to *n*-type behavior which the thermopower activation energy cannot account for. This can be understood by the ''crowding'' of the fixed concentration of hopping sites ($Mn^{3+}+Mn^{4+}$) by electrons when the material is *p* type. This leads to greater activation energies for hopping due to increased electron-electron repulsion, and has been concluded in other oxides.[17] As the concentration of Mn^{4+} increases with oxygen superstoichiometry, the concentration of ''empty'' sites increases, there is less electron-electron repulsion, and lower activation energy ensues. Why the activation energy change should be as rapid as it is at the *p*-*n* transition is not clear.

The consistency of the measurements of the thermopower and resistivity pre-exponential can be compared by computing the value of $c(1-c)$ from each. Figure 9 computed from the data of Table I, shows at least a qualitative correspondence. Figure 10 shows the values of c and $(1-c)$ whose product is interpolated to give the peak in the $c(1-c)$ curve from Q in Fig. 9.

The value $c(1-c)$ is calculated from the flat regions of the thermopower. For $c(1-c)$ from the pre-exponential, recall the pre-exponent is $\rho_0/T=(e^2Nc(1-c)\nu_D d^2/k)^{-1}$, which is the product of the carrier containing sites c, and the empty sites $(1-c)$, the Debye frequency (jump frequency) ν_D, the square of the jump distance d, and the usual physical constants. $N=[Mn^{3+}]+[Mn^{4+}]$ is the sum of the concentrations of the species of mixed valence $c=[Mn^{3+}]/N$ and $1-c=[Mn^{4+}]/N$.

The Debye frequency is given by the Debye temperature and this changes as a function of oxygen partial pressure. The density of octahedrally coordinated hopping sites $N_{oct}=16/a_0^3$ where the lattice constant $a_0\sim 8.35$ Å and for the purposes of this estimation, is nearly constant, $d\sim N_{oct}{}^{-1/3}$. Since $c(1-c)$ was calculated from the thermopower assum-

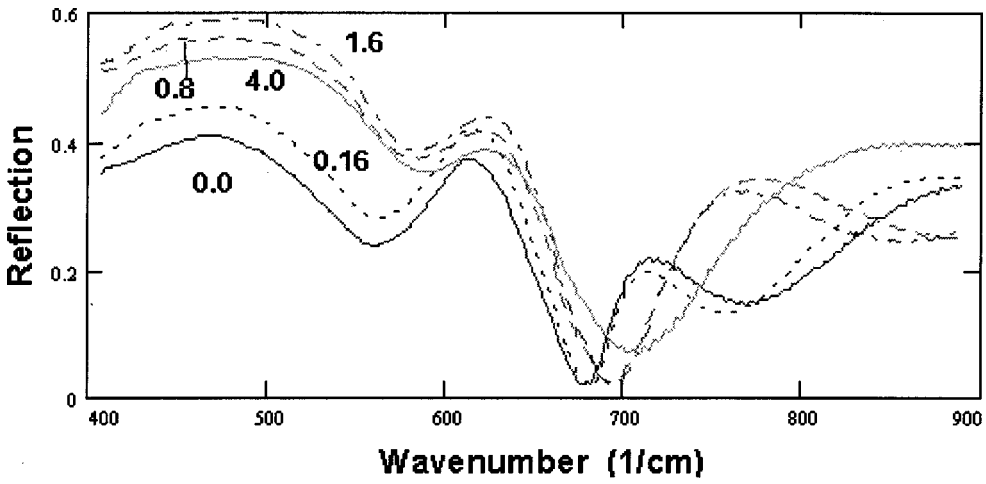

FIG. 8. IR reflection (0 to 1) data showing maxima and minima between 400 and 700 cm^{-1}, which are caused by IR active vibrations. Thickness fringes occur greater than 700 cm^{-1}. Restrahlen peaks occur near 490 and 630 cm^{-1}. Note the shift to higher wave number with increasing oxygen.

TABLE III. Restrahlen and Raman maxima trend with oxygen partial pressure during sputtering of films from FTIR data and Debye temperature from the Schnakenberg relation. $V1$ and $V2$ are the IR vibrations visible in Fig. 8 and $R1$ and $R2$ are the two highest energy Raman shifts of Fig. 7.

	$V1$ cm^{-1}	$V2$ cm^{-2}	$R1$ cm^{-1}	$R2$ cm^{-1}	θ_D (K)[a]
0 mTorr	613	469	641.7	517.3	552
0.16 mTorr	616	476	643.7	520.5	619
0.4 mTorr	…	…	…	…	625
0.8 mTorr	620	476	651.1	533	635
1.6 mTorr	623	482	652.8	533.6	681
4 mTorr	623	491	653	533–540	741

[a]Data from Table I.

ing hopping between only one set of multivalent cations, N given from Eq. (6) will be assumed for calculation of $c(1-c)$ from the pre-exponent $N=(0.48+0.637)N_{\text{oct}}/2$. These results are shown in Fig. 9 where it can be seen that the drop at the p to n transition is preserved, and, the two values are approaching each other.

Although the agreement is not perfect, there is qualitative agreement in that at the p to n transition, which happens between 0.4 to 0.8 mTorr, both $c(1-c)$ and the pre-exponent decrease. This happens because at the transition, $c/(1-c)$ goes from greater to less than unity as Q goes from positive to negative, and $c(1-c)$ is a maxima, since the conductivity pre-exponent is maximized when the carrier concentration equals the concentration of vacant sites, $[Mn^{3+}]=[Mn^{4+}]$.

An estimate of the polaron mobility provides evidence that stoichiometric material is made by sputtering somewhere between 0.16 to 0.8 mTorr oxygen partial pressure. According to Yokoyama, the thermopower for a stoichiometric composition of this material is $Q\sim 25$ uV/K. Linearly interpolating the data for the sputtered samples, this corresponds to an oxygen partial pressure of ~0.4–0.6 mTorr. At 300 K the material deposited at 0.4 mTorr has a resistivity of ~1000 Ω cm. Using Eq. (5) with $X=0.5$, and that $((1-X)/2)N_{\text{oct}}$ is the density of Mn^{4+} ''holes'' with $a_0=8.35$ Å, the hole mobility we calculate to be $\mu\sim 1\mu$ cm^2/V s. This compares very well with the mobilities of other manganate spinels studied in bulk form, for example, nickel manganate at 0.77 μ cm^2/V s at 300 K.[18]

Finally, the observation which attests to the trend of the Debye temperature to increase with the oxygen partial pressure as computed from the resistivity, is that both the observable Raman active vibrations and infrared (IR) active vibrations (restrahlen peaks in reflection) shift to higher frequencies with oxygen partial pressure. This suggests that as this oxide passes from sub-stoichiometric in oxygen to super stoichiometric in oxygen, the lattice stiffens, since the Debye temperature is an indicator of the lattice stiffness.

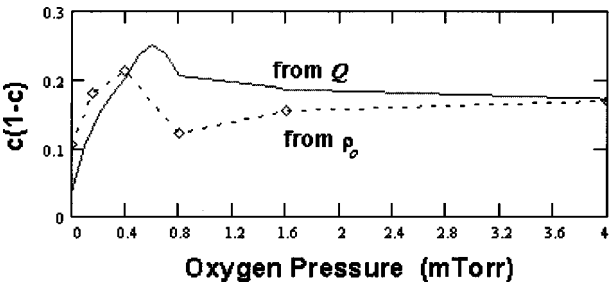

FIG. 9. Calculation of $c(1-c)$ from thermopower and also from the conductivity preexponent. There is a change in the sign of the slope between 0.16 and 0.8 mTorr, consistent with the transition in carrier type. The peak in $c(1-c)$ computed from Q is interpolated from the data of Fig. 10.

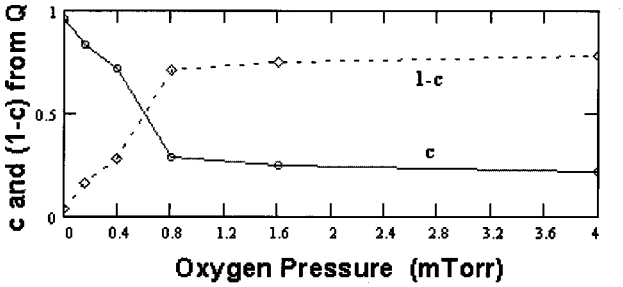

FIG. 10. The c and $(1-c)$ computed from the thermopower Q of Table I.

VII. CONCLUSIONS

We conclude:

(1) Yokoyama's conclusion that Mn^{3+} and Mn^{4+} should be the multivalent cation influencing the transport properties is supported by this study.

(2) This material undergoes a p-n transition with oxygen partial pressure during sputtering due to a gradual change from an oxygen sub-stoichiometric state to a super-stoichiometric state, which causes the ratio of Mn^{3+} to Mn^{4+} to decrease. Since energy dispersive spectroscopy (EDS) shows that the relative concentrations of the transition metals involved vary by less than 2% from the target composition in all cases, and XRD shows all films are single phase spinel, the effect is due to oxidation.

(3) Transport is by small polaron hopping.

(4) The thermopower measurement technique for films, utilizing large temperature differences, produces mobility and thermopower results that are consistent with published data on these oxides.

(5) The trends in resistivity computed from the Schnakenberg relation are consistent with the trends in the thermopower, and trends in the Raman and IR active vibrations.

(6) The Debye frequency, and Raman and restrahlen IR vibrations shift to higher frequency with oxygen stoichiometry, implying a stiffening of the lattice.

ACKNOWLEDGMENTS

The authors wish to express deepest thanks to Servo Corporation of America and The Strategic Partnership for Industrial Resurgence Program (SPIR) at The State University of New York at Stony Brook Engineering Department for jointly supporting this work.

[1] I. T. Sheftel, A. I. Zaslavskii, E. V. Kurlina, G. N. Tekster Provryakova, Sov. Phys. Solid State **3**, 1978 (1962).
[2] N. F. Mott, *Metal-Insulator Transitions*, 2nd ed. (Taylor and Francis, London, 1990).

[3] N. F. Mott, *Conduction in Non-Crystalline Materials* (Clarendon, Oxford, 1987).
[4] N. F. Mott and E. A. Davis, *Electronic Processes in Non-Crystalline Materials* (Clarendon, Oxford, 1987).
[5] A. K. Cheetham and P. Day, *Solid State Chemistry: Techniques* (Clarendon, Oxford, 1987).
[6] *Polarons in Ionic Crystals and Polar Semiconductors*, edited by J. T. Devrees (North-Holland, Amsterdam, 1971), Chap. VII, p. 679, review by H. G. Reick.
[7] J. Topfer *et al.*, MRS Bull. **29**, 225 (1994).
[8] T. Yokoyama *et al.*, Jpn. J. Appl. Phys., Part 1 **35**, 5775 (1996).
[9] J. Schnakenberg, Phys. Status Solidi **28**, 623 (1968).
[10] *Thermometric Sensor Handbook* (Thermometrics, Inc., 1987).
[11] J. A. Becker, C. B. Green, and G. L. Pearson, Bell Syst. Tech. J. **26**, 1970 (1947).
[12] G. Bossom, F. Gutman, and L. M. Simmons, J. Appl. Phys. **21**, 1267 (1950).
[13] S. Baliga, A. L. Jain, and W. Zachovsky, Appl. Phys. A: Solids Surf. **50**, 473 (1990).
[14] S. Baliga and A. L. Jain, Mater. Lett. **8**, 175 (1989).
[15] S. Baliga and A. L. Jain, Mater. Lett. **11**, 226 (1991).
[16] T. E. Whall, K. K. Yeung, and Y. G. Proykove, Philos. Mag. B **S4**, 505 (1986).
[17] I. K. Naik and T. Y. Tien, Phys. Chem. Solids **39**, 311 (1978).
[18] J. Topfer *et al.*, Phys. Status Solidi A **134**, 405 (1992).